

Investigation of High Energy Behaviour of HERA Data

A. Luszczak ¹ and H. Kowalski ²

¹ *T.Kosciuszko, Cracow University of Technology, Institute of Physics, st. Podchorazych 1,
30-084 Krakow, Poland*

² *Deutsches Elektronen-Synchrotron DESY, Berlin and Hamburg, Germany*

Abstract

We analyse the high precision HERA F_2 data in the low- x , $x < 0,01$, and very-low- x , $x < 0.001$, regions using λ -fits. λ is a measure of the rate of rise of F_2 defined by $F_2 \propto (1/x)^\lambda$. We show that λ determined in these two regions, at various Q^2 values, is systematically smaller in the very-low- x region as compared to the low- x region. We discuss some possible physical interpretations of this effect.

1 Introduction

From the first measurements of HERA it was already known, that the rise of F_2 with diminishing x can be described by a simple parametrisation; $F_2 \propto (1/x)^\lambda$, where the parameter λ is a function of Q^2 [1]. The observed values of λ are increasing with Q^2 , at $Q^2 = 0.35 \text{ GeV}^2$ λ is about 0.1 and at $Q^2 = 250 \text{ GeV}^2$ λ is about 0.4.

Before HERA, it was expected that the virtual photon-hadron cross section, σ^{γ^*p} , should rise with energy in a similar way as the hadronic cross sections. The value of the exponent λ , obtained from the analysis of hadron-hadron scattering data, was about 0.08 and it was expected that this value should be universal, i.e. independent of the type of reaction and of Q^2 [2]. The physical motivation behind this expectation relied on the fact that in the low- x region the interaction time is very long (in the proton rest frame it is given by $1/(m_p x)$) and therefore the incoming virtual photon has enough time to get "dressed", i.e. to behave like a hadron.

The observation of λ values, which were sizeably larger than 0.08 and were rising with Q^2 was a clear sign that F_2 is measuring a fundamental partonic process, since in QCD the phase space for gluon emission grows quickly with increasing Q^2 and decreasing x . One of the possible physical interpretations of the parameter λ is that it is a rate of gluon emissions per unit of rapidity, see e.g. [1].

Long before HERA, it was known from QCD, that the gluon density, in the double asymptotic limit of $x \rightarrow 0$ and $Q^2 \rightarrow \infty$, should behave as

$$xg(x, Q^2) = \exp \sqrt{C \ln \frac{\ln Q^2/\Lambda}{\ln Q_0^2/\Lambda} \ln 1/x}$$

where C is a known constant and Λ is the QCD scale [3,4], i.e. F_2 grows with decreasing x and increasing Q^2 . The same double asymptotic limit is also derived in BFKL [5], see e.g. the discussion in [6].

In the HERA region, i.e. well below the double asymptotic domain, the data can be well described, including the λ behaviour, by fitting the starting density distributions of quarks and gluons with DGLAP. The final, high precision HERA data has shown, however, that something is missing in these fits [7]. There is now a growing consensus that the observed discrepancies are due to the BFKL effects in the low- x region, where DGLAP evolution should not be valid, see e.g. [8].

Before HERA, the standard prediction of BFKL was that F_2 , in the low- x region, should be dominated by the leading singularity, i.e. $F_2 \propto (1/x)^\omega$, with $\omega \approx 0.3$ (in NLO) [9,10]. This prediction, obtained from the evaluation of the BFKL amplitude in the Mellin space using the saddle point approximation, was in clear contradiction with the observed increase of the exponent λ with Q^2 . In an alternative approach, Lev Lipatov proposed [11] to introduce the infrared cutoff, which leads to a discrete BFKL pole structure when the running of the strong coupling constant, α_s , is taken into account. It was then shown that the combined effect of these poles reproduces the observed behaviour of the parameter λ [12] and provides

an excellent fit to the high precision HERA data, in the very low x region, $x < 0.001$ and $Q^2 > 6 \text{ GeV}^2$ [13].

The investigation of ref. [13] led to an unexpected result: the F_2 data were described by the sub-leading poles only. Moreover, it was found that the leading pole has to be in the saturation or even non-perturbative region, so that its contribution to the investigated region had to be negligible. The second pole, which is leading for $Q^2 > 6 \text{ GeV}^2$, has $\omega \approx 0.14$, i.e. a substantially lower value than the values of the observed λ 's in this Q^2 region. This result leads to the expectation that at very low x one could observe a substantially lower values of λ .

Another interesting feature of HERA data was pointed out in ref. [14], where it is shown that the logarithmic linearity of HERA data, $\log F_2 \propto \lambda \log(1/x)$, has to break down. The argument is simple; the γp cross section, $\sigma^{\gamma p} = 4\pi\alpha F_2/Q^2$, is smaller for larger Q^2 but it rises faster with diminishing x . Therefore, there is a cross over point, at about $x = 10^{-8}$, where the γp cross sections for larger Q^2 's are becoming larger than the cross sections for smaller Q^2 . This is a contradiction because the cross section of a smaller projectile cannot be larger than the cross section of a larger one (the transverse size of the incoming photon is given by $1/Q^2$).

All this provides a motivation to refit the HERA high precision data [7] with the parametrisation, $F_2 \propto (1/x)^\lambda$, using the full set of statistical and correlated systematic errors. We want to see whether the logarithmic linearity still holds or whether we can see any change in the rate of rise, λ , with diminishing x .

2 Description of fits

We determine the λ parameter from a fit of the function $F_2 = A(1/x)^\lambda$ to the final, high precision H1 and ZEUS data, measured at HERA [7]. Here, A is a normalisation constant dependent on Q^2 . The fits are made in the range $x < 0.01$ and $x < 0.001$, for each Q^2 value separately, with $0.3 < Q^2 < 250 \text{ GeV}^2$. The final data are given as reduced cross sections, which are connected to F_2 and F_L by:

$$\sigma_{red} \approx F_2 - \frac{y^2}{Y_+} F_L,$$

with $Y_+ = 1 + (1 - y)^2$, where y denotes the inelasticity parameter. In the selected kinematic region, the contribution of the structure function F_3 can be neglected. Following the discussion of the properties of F_L in the H1 papers [15, 16], we assume that F_L is proportional to F_2 . This is also in agreement with the ZEUS results, see e.g. [17, 18]. We have then

$$F_2 = \frac{\sigma_{red}}{1 - \frac{y^2 R}{Y_+(1+R)}},$$

where $R = F_L/(F_2 - F_L)$. The evaluation of F_L shows that the ratio R is only weakly dependent on x and Q^2 , especially in the kinematic region of the present investigation,

$0.01 < y < 0.8$ [16, 17]. Thus we assumed $R = 0.25$, in agreement with data, the QCD DGLAP predictions and the dipole models [19–22].

The results of the fits are given in Tables 1 and 2. Table 1 shows the values of λ constant with its error $\delta\lambda$ for two low- x regions, $x < 0.01$ and $x < 0.001$. Table 2 show the values of A constant and its errors in the same x regions. In both Tables we give also the values of χ^2 of the individual fits divided by the number of degrees of freedom, N_{df} . (The values of χ^2 's and N_{df} 's are the same in both Tables as the constants λ and A are determined in the same fit.) The number of degrees of freedom is given by the number of experimental points used in the fit, at a given Q^2 value, lowered by the number of parameters of the fit, i.e. 2.

Table 1 shows that the fits are of good quality, as the average value of χ^2/N_{df} is 1.05, at $x < 0.01$. The fits in the $x < 0.001$ region are of similar quality. In our analysis we concentrate on the region between $2.7 < Q^2 < 45 \text{ GeV}^2$, for which the F_2 measurements in the low- x and the very-low- x region overlaps and are different. In this region, the error of λ , which includes the statistical and correlated systematic uncertainties, is around 2 % in the low- x and typically twice as big in the very-low- x region.

As is well known, the rate of rise, λ , increases clearly with the increase of Q^2 , see Fig. 1. The new observation of this investigation is that the values of λ are systematically lower in the $x < 0.001$ region as compared to the $x < 0.01$ region. In Figure 2 we compare the value of λ in the two regions and we see that, although the differences for the individual fits are only of the order of one standard deviation, almost all of the fits show lower values of λ in the very low x region.

In Fig. 3, 4, 5, 6, 7, 8 and 9 we compare the fitted curves to the corresponding data in all Q^2 regions, between 2.7 and 45 GeV^2 . The curves are drawn with the values of the constants λ and A given in Tables 1 and 2. The full line shows the fit in the region $x < 0.01$ and the dashed one the fit to the region $x < 0.001$. The curves are drawn in a larger region than the fit are performed, to emphasise the systematic differences between them. The figures show quite clearly that the dashed lines are almost always below the full lines in the region of very small $x < 0.001$. On the opposite end, around $x \approx 0.01$, the full line is almost always above the dashed one. Since the figures are drawn on a double logarithmic scale (and are relatively large) it is possible to see, even clearly in some cases, a slight "bowing" of data due to a systematic decrease of λ at smaller x values, seen in Fig. 2 and Table 1.

To check the dependence of our results on the assumed value of R , we show in Fig. 10 the differences between the values of λ determined in the low x and very low x region, $\Delta\lambda = \lambda_{x < 0.01} - \lambda_{x < 0.001}$, assuming $R = 0.2$, $R = 0.25$ and $R = 0.3$. Fig. 10 shows that the rate of rise λ remains sensitive to the assumed value of R , in spite of the cut on the variable $y = 0.8$. Since the value of R was determined as $R = 0.23 \pm 0.04$ [16], the main result of this paper remains valid even in the extreme case of $R = 0.3$.

3 Discussion and Conclusions

We have confirmed that the simple phenomenological function, $F_2 \propto (1/x)^\lambda$, fits very well the high precision HERA data in the low x region, $x < 0.01$, at all Q^2 values between $0.3 < Q^2 < 250 \text{ GeV}^2$. Moreover, we have shown that this is also true for the very low x region, $x < 0.001$. The new result of this investigation is that the rate of rise, λ , determined in the two regions, indicate that λ is systematically smaller in the very low x region as compared to the low x region, for $Q^2 > 6 \text{ GeV}^2$. This result is obtained due to the high precision of the latest HERA data [7] whereas the earlier investigations concluded that the power λ is not dependent on x , within the experimental errors, see e.g. ref. [23]. In a more recent investigation, [15], it was noticed, although indirectly, that λ values may diminish with decreasing x , in agreement with the present investigation.

This observation may indicate the onset of BFKL behaviour in the very low x region, $x < 0.001$, $Q^2 > 6 \text{ GeV}^2$, in agreement with the analysis of ref. [13]. The analysis has shown that the BFKL gluon density describe data very well in this region and that the dominant contribution is provided by the second pole, which has $\omega \approx 0.14$, a value which is substantially smaller than the λ value observed in this region, see Table 1. Note that the evaluation of ref. [13] does not allow a quantitative estimate of the expected change of the power λ between the low x and very low x regions, as the high quality of BFKL description was obtained only in the second region.

The observation of a systematic decrease of λ with diminishing x could also indicate that the double asymptotic region, in which $F_2 \approx \exp c\sqrt{\ln(1/x)}$, may be only few decades away from the $x < 0.001$ region observed at HERA.

In any case, our observation that the value of the exponent λ decreases at small values of x , indicates that measurements at the future ep colliders, like VHEeP or LHeC [24, 25] will become exciting, as they will approach the high energy limit of the virtual photon-hadron cross sections, where DGLAP and BFKL meets [6] and the confinement effects should become simple [26].

Acknowledgments

We are grateful to Allen Caldwell and Sasha Glazov for very useful discussions and suggestions for improvements.

References

- [1] J. Bartels and H. Kowalski, Eur.Phys.J. **C19** (2001) 693-708.
- [2] A. Donnachie and P.V. Landshoff, Nucl.Phys. **B 244** (1984) 322 and Phys. Lett. **B 296** (1992) 227.
- [3] A. De Rujula, S.L. Glashow, H.D. Politzer, S.B. Treiman, F. Wilczek and A. Zee, Phys. Rev. **10** (1974) 1649.
- [4] V.N. Gribov and L.N. Lipatov, Sov. Nucl. Phys. **15** (1972) 438
G. Altarelli and G. Parisi, Nucl. Phys. **B126** (1977) 298
Yu. L. Dokshitzer, Sov. Phys. JETP **46** (1977) 46
- [5] I. I. Balitsky and L. N. Lipatov, Sov. J. Nucl. Phys. **28** (1978) 822; E. A. Kuraev, L. N. Lipatov and V. S. Fadin, Sov. Phys. JETP **44** (1976) 443; V. S. Fadin, E. A. Kuraev and L. N. Lipatov, Phys. Lett. B **60** (1975) 50.
- [6] H. Kowalski, L.N. Lipatov, D. A. Ross, Eur. Phys. J **C76** (2016) 3
- [7] H. Abramowicz *et al.* [H1 and ZEUS Collaborations], Eur. Phys. J. **C75** (2015) 580.
- [8] R. D. Ball, V. Bertone, M. Bonvini, S. Marzani, J. Rojo, L. Rottoli. Eur.Phys. J. **C78** (2018) no.4, 321.
- [9] J. R. Forshaw and D. A. Ross, Quantum Chromodynamics and the Pomeron, Cambridge University Press, 1997.
- [10] G. P. Salam, JHEP **9807** (1998) 019.
- [11] L. N. Lipatov, Sov. Phys. JETP **63** (1986) 904.
- [12] H. Kowalski, L.N. Lipatov, D. A. Ross, and G. Watt Eur. Phys. J **C70** (2010) 983; Nucl. Phys **A854** (2011) 45.
- [13] H. Kowalski, L.N. Lipatov, D. A. Ross, O. Schulz, Eur. Phys. J **C77** (2017) 7777.
- [14] A. Caldwell and M. Wing, Eur.Phys.J. **C76** (2016) 463.
- [15] F. D. Aaron et al. [H1 Collaboration], Eur.Phys.J. **C71** (2011) 1579.
- [16] V. Andreev et al. [H1 Collaboration], Eur.Phys.J.C **74** (2014) 2814.
- [17] H. Abramowicz et al. [ZEUS Collaboration], Phys.Rev. **D 90** (2014) 072002.
- [18] A. Caldwell, “Behavior of $\sigma^{\gamma p}$ at Large Coherence Lengths”, arXiv:**0802.0769** (2008).
- [19] H. Kowalski and D. Teaney, Phys. Rev. **D 68**, 114005.
- [20] C. Ewerz and O. Nachtmann, Phys. Lett. **B 648** (2007) 279 [hep-ph/0611076].

- [21] C. Ewerz and O. Nachtmann, *Annals Phys.* **322** (2007) 1670 [hep-ph/0604087].
- [22] A. Luszczak and H. Kowalski, *Phys.Rev.* **D95** (2017) 014030.
- [23] C. Adloff et al. [H1 Collaboration], *Phys. Lett.* **B520** (2001) 183.
- [24] A. Caldwell and M. Wing , “VHEeP: A very high energy electron proton collider based on proton-driven plasma wakefield acceleration”, arXiv:**1509.00235** (2015).
- [25] LHeC Study Group, J L Abelleira Fernandez et al 2012 *J. Phys. G: Nucl. Part. Phys.* **39** 075001.
- [26] R.P.Feynman, *Photon-Hadron Interactions*, W.A.Benjamin, Inc.Publisher 1972.

Q^2	$x < 0.01$				$x < 0.001$			
	λ	$\delta\lambda$	N_{df}	χ^2/N_{df}	λ	$\delta\lambda$	N_{df}	χ^2/N_{df}
0.35	0.110	0.008	10	0.850	0.110	0.0081	10	0.850
0.4	0.082	0.009	7	0.915	0.082	0.009	7	0.915
0.5	0.100	0.009	7	0.768	0.100	0.009	7	0.768
0.65	0.121	0.011	7	0.813	0.121	0.011	7	0.813
0.85	0.150	0.014	7	0.759	0.150	0.014	7	0.759
1.2	0.133	0.013	8	2.074	0.133	0.013	8	2.074
1.5	0.142	0.009	10	1.741	0.142	0.009	10	1.741
2	0.159	0.007	10	1.246	0.159	0.007	10	1.246
2.7	0.169	0.005	12	1.745	0.168	0.007	10	1.462
3.5	0.173	0.004	18	1.391	0.168	0.007	16	1.485
4.5	0.189	0.004	13	1.908	0.192	0.008	10	2.347
6.5	0.200	0.003	29	0.990	0.189	0.008	25	1.002
8.5	0.208	0.004	34	1.252	0.192	0.009	27	1.047
10	0.226	0.007	5	1.005	0.205	0.024	2	0.518
12	0.215	0.005	33	1.016	0.202	0.009	24	0.715
15	0.237	0.003	32	1.217	0.219	0.010	21	1.303
18	0.242	0.003	11	0.401	0.234	0.012	6	0.358
22	0.258	0.007	11	0.961	0.241	0.018	6	0.601
27	0.267	0.004	10	0.632	0.267	0.020	5	0.136
35	0.280	0.003	35	1.144	0.251	0.021	13	1.759
45	0.292	0.004	33	0.877	0.263	0.057	5	1.085
60	0.313	0.005	32	1.274				
70	0.332	0.009	10	0.812				
90	0.321	0.007	27	0.925				
120	0.352	0.008	31	0.506				
150	0.339	0.011	17	1.101				
200	0.373	0.010	16	0.545				
250	0.417	0.014	13	0.727				

Table 1: The results for the λ constant obtained from the fits of the function $F_2 = A(1/x)^\lambda$ to the final, high precision H1 and ZEUS data at all Q^2 values, in the low- x and very-low- x regions, $x < 0.01$ and $x < 0.001$. Note that below $Q^2 < 2.7$ GeV² there are no differences between the two regions.

Q^2	$x < 0.01$				$x < 0.001$			
	A	δA	N_{df}	χ^2/N_{df}	A	δA	N_{df}	χ^2/N_{df}
0.35	0.0957	0.008	10	0.850	0.0957	0.008	10	0.850
0.4	0.143	0.013	7	0.915	0.143	0.014	7	0.915
0.5	0.136	0.013	7	0.768	0.136	0.013	7	0.768
0.65	0.133	0.015	7	0.813	0.133	0.015	7	0.813
0.85	0.120	0.018	7	0.759	0.120	0.018	7	0.759
1.2	0.170	0.022	8	2.074	0.170	0.022	8	2.074
1.5	0.180	0.016	10	1.741	0.184	0.016	10	1.741
2	0.172	0.012	10	1.246	0.172	0.012	10	1.246
2.7	0.179	0.008	12	1.745	0.181	0.012	10	1.462
3.5	0.195	0.007	18	1.391	0.203	0.012	16	1.485
4.5	0.191	0.007	13	1.908	0.186	0.0013	10	2.347
6.5	0.201	0.006	29	0.990	0.221	0.015	25	1.002
8.5	0.211	0.007	34	1.252	0.234	0.016	27	1.047
10	0.192	0.010	5	1.005	0.226	0.044	2	0.518
12	0.225	0.008	33	1.016	0.247	0.018	24	0.715
15	0.202	0.005	32	1.217	0.232	0.019	21	1.303
18	0.208	0.005	11	0.401	0.218	0.021	6	0.358
22	0.197	0.010	11	0.961	0.223	0.030	6	0.601
27	0.196	0.005	10	0.632	0.195	0.029	5	0.136
35	0.193	0.005	35	1.144	0.239	0.037	13	1.759
45	0.190	0.005	33	0.877	0.234	0.096	5	1.085
60	0.179	0.005	32	1.274				
70	0.164	0.009	10	0.812				
90	0.188	0.008	27	0.925				
120	0.163	0.008	31	0.506				
150	0.183	0.011	17	1.101				
200	0.158	0.008	16	0.545				
250	0.129	0.010	13	0.727				

Table 2: The results for the A constant obtained from the fits of the function $F_2 = A(1/x)^\lambda$ to the final, high precision H1 and ZEUS data at all Q^2 values, in the low- x and very-low- x regions, $x < 0.01$ and $x < 0.001$. Note that below $Q^2 < 2.7$ GeV² there are no differences between the two regions.

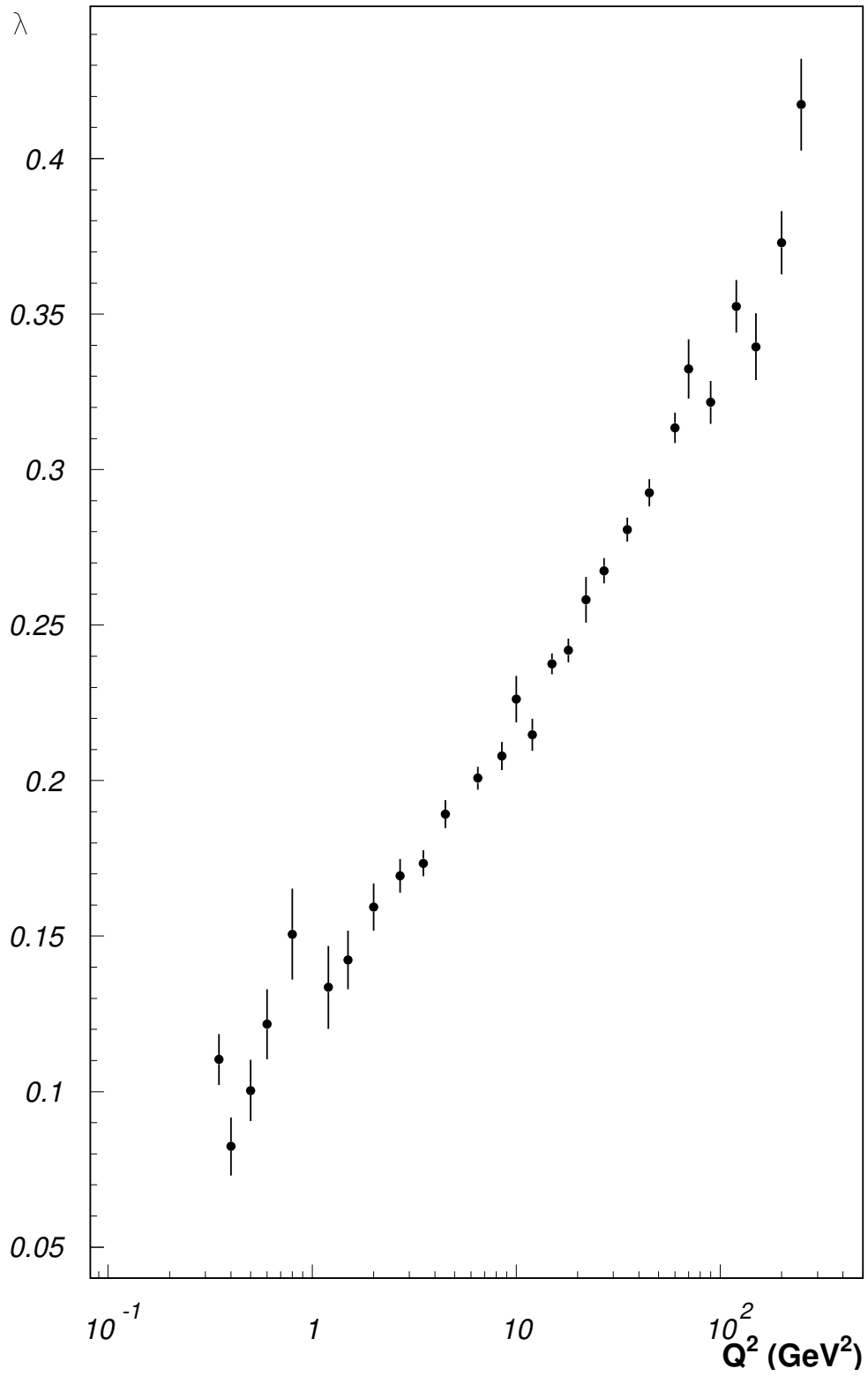


Figure 1: The power λ as determined from the fits in the $x < 0.01$ region, at all accessible Q^2 values, Table 1.

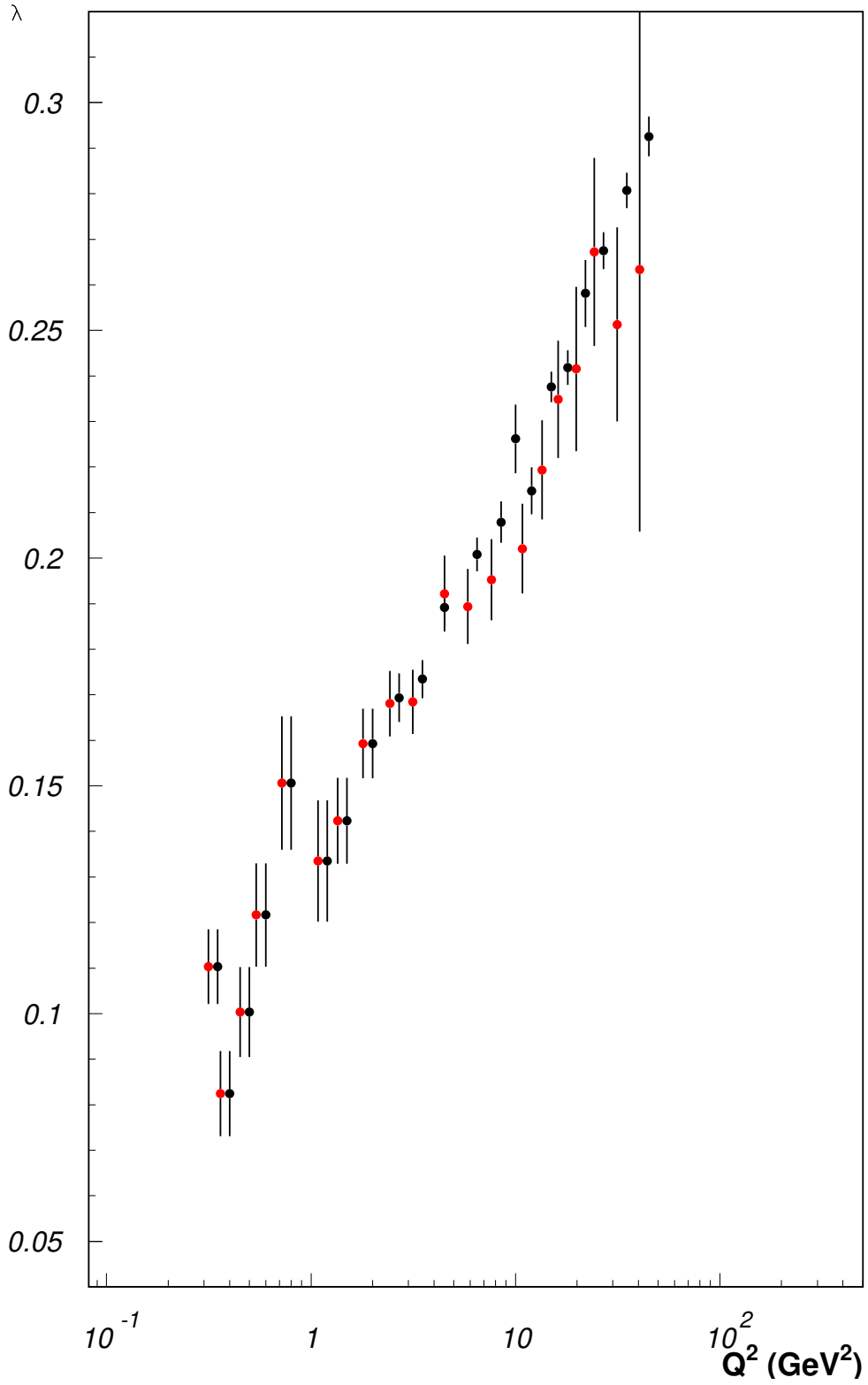


Figure 2: Comparison of the results of the λ -fit in the low- x , $x < 0.01$, and very-low- x , $x < 0.001$, regions. Only points determined with differing data are shown, see Table 1.

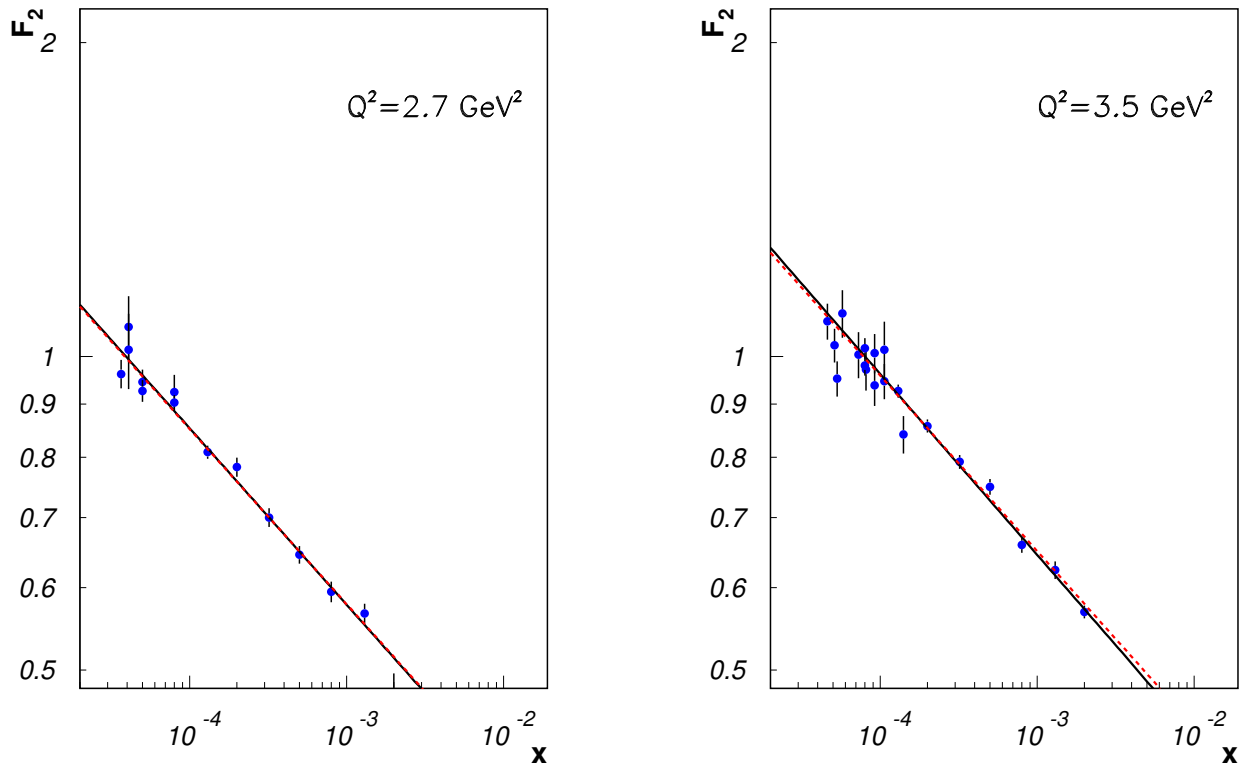


Figure 3: The fitted curves, $F_2 \propto (1/x)^\lambda$, are shown together with the data at indicated Q^2 values. The full line shows the fit in the range $x < 0.01$, the dotted line in the range $x < 0.001$. The dots show the data with error bars given by the statistical and systematical errors added in quadrature. In the fit, all correlations of errors were taken into account.

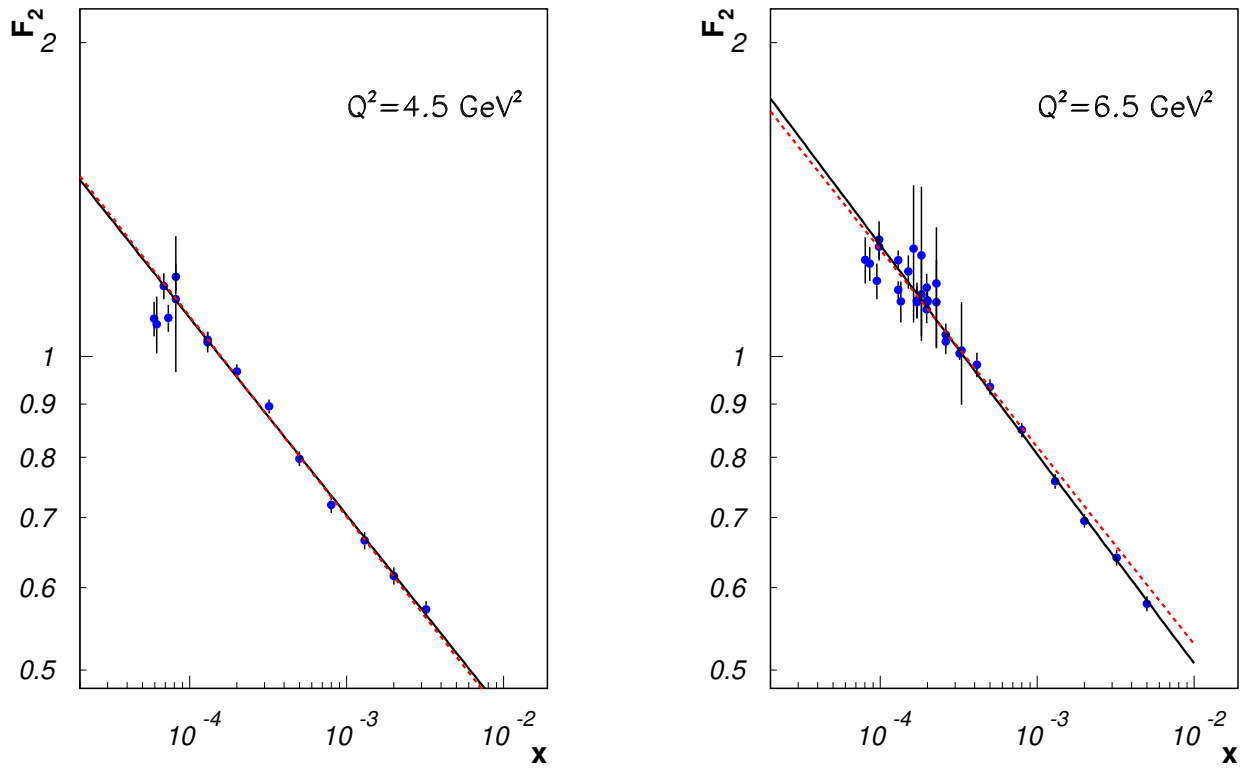


Figure 4: The fitted curves, $F_2 \propto (1/x)^\lambda$, are shown together with the data at indicated Q^2 values. The full line shows the fit in the range $x < 0.01$, the dotted line in the range $x < 0.001$. The dots show the data with error bars given by the statistical and systematical errors added in quadrature. In the fit, all correlations of errors were taken into account.

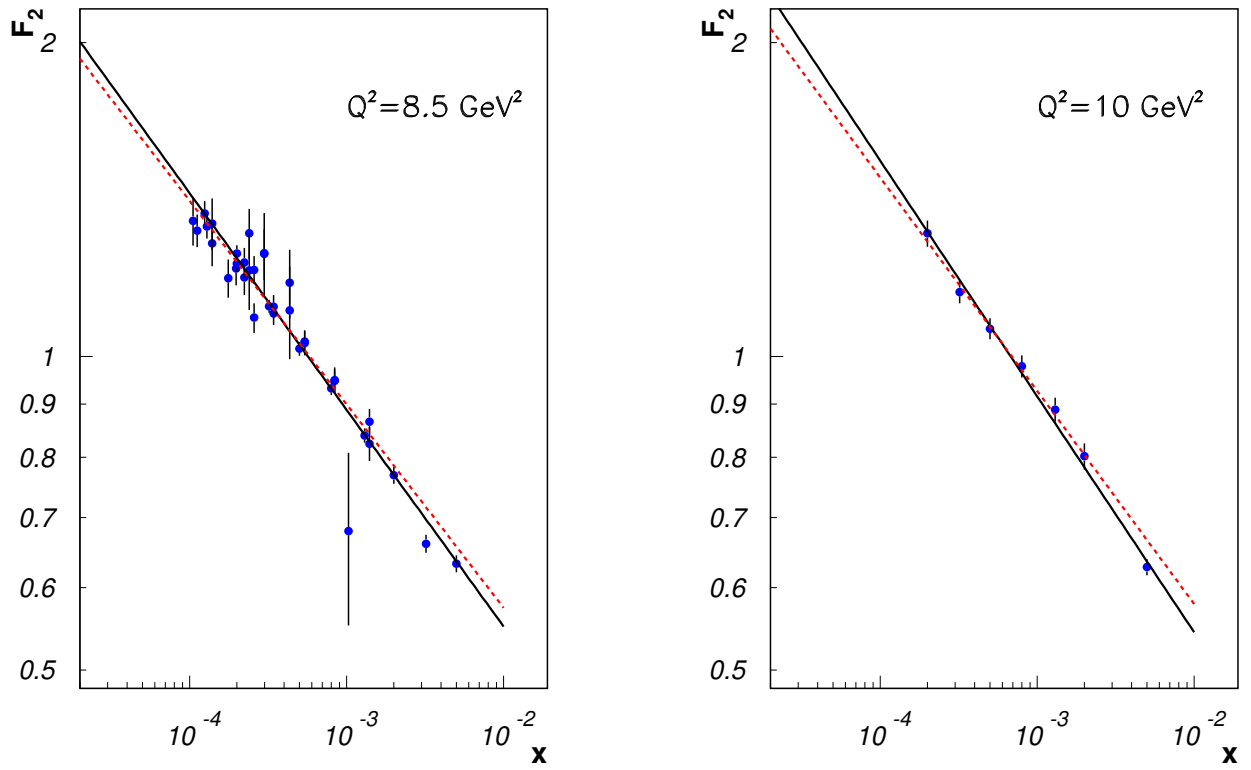


Figure 5: The fitted curves, $F_2 \propto (1/x)^\lambda$, are shown together with the data at indicated Q^2 values. The full line shows the fit in the range $x < 0.01$, the dotted line in the range $x < 0.001$. The dots show the data with errors bars given by the statistical and systematical errors added in quadrature. In the fit, all correlations of errors were taken into account.

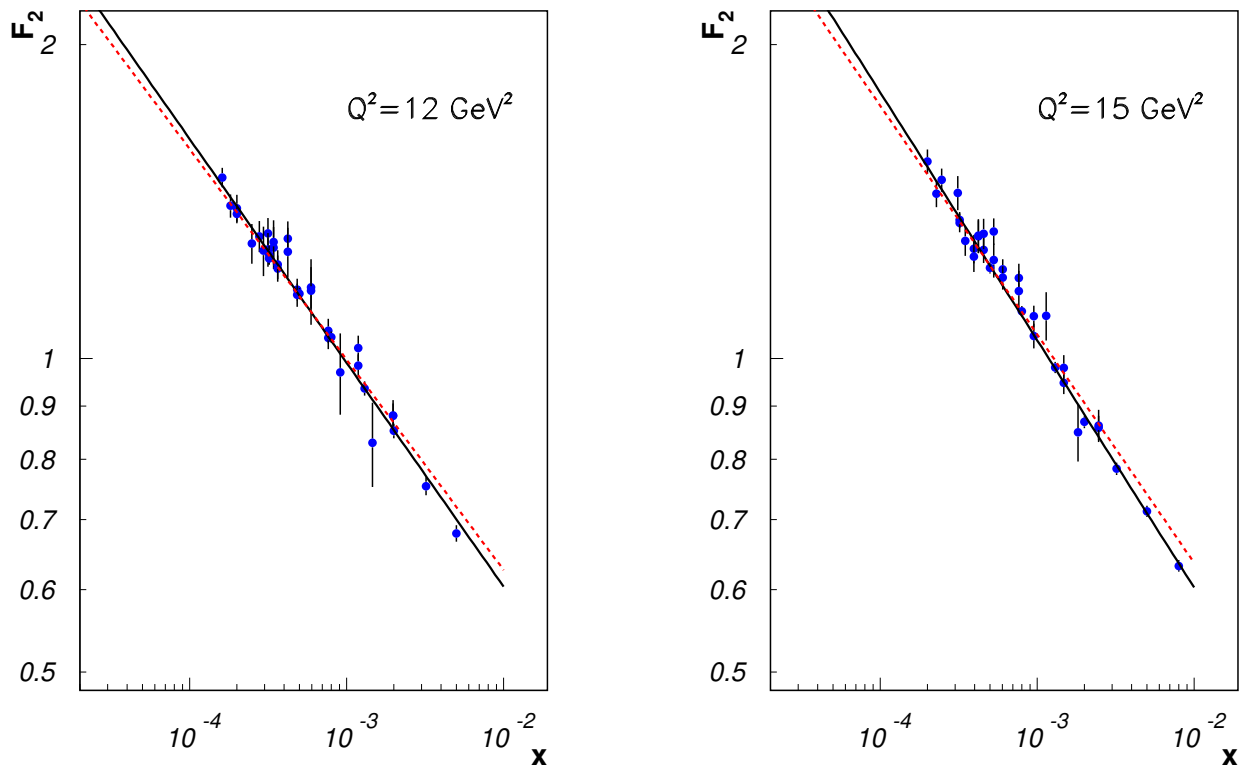


Figure 6: The fitted curves, $F_2 \propto (1/x)^\lambda$, are shown together with the data at indicated Q^2 values. The full line shows the fit in the range $x < 0.01$, the dotted line in the range $x < 0.001$. The dots show the data with error bars given by the statistical and systematical errors added in quadrature. In the fit, all correlations of errors were taken into account.

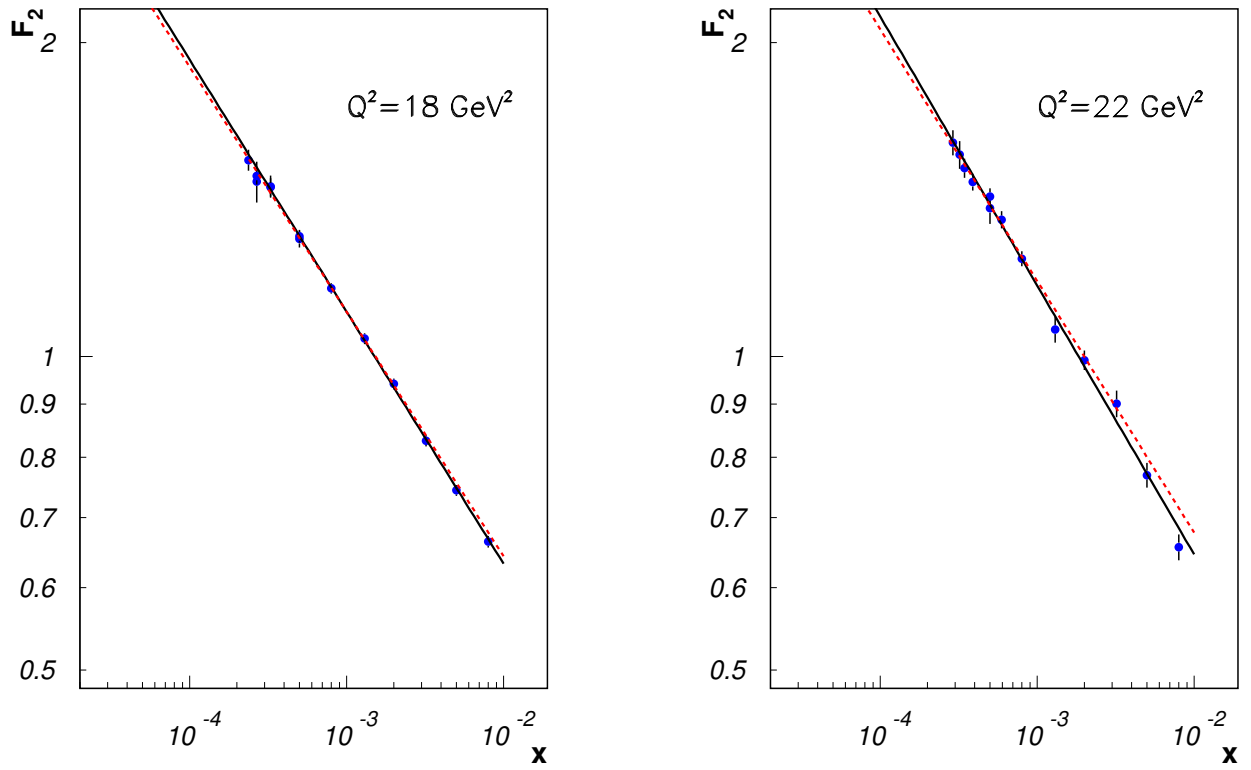


Figure 7: The fitted curves, $F_2 \propto (1/x)^\lambda$, are shown together with the data at indicated Q^2 values. The full line shows the fit in the range $x < 0.01$, the dotted line in the range $x < 0.001$. The dots show the data with errors bars given by the statistical and systematical errors added in quadrature. In the fit, all correlations of errors were taken into account.

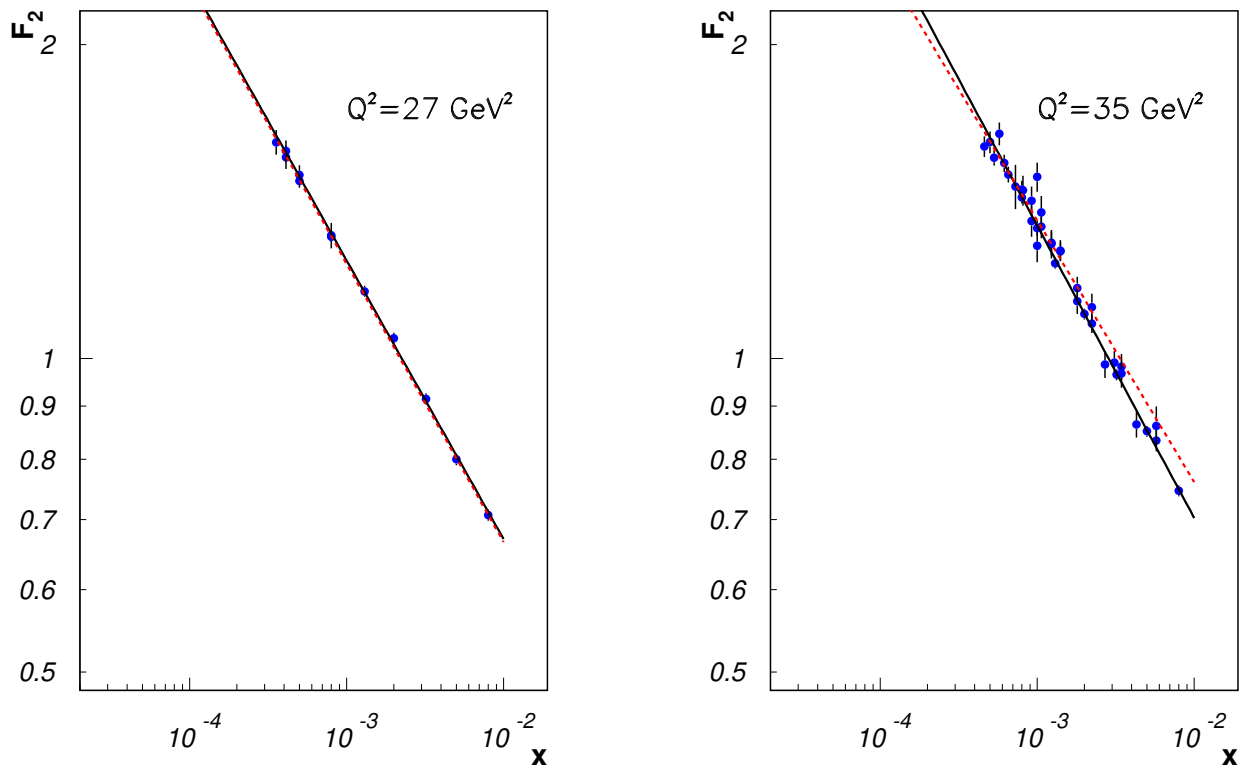


Figure 8: The fitted curves, $F_2 \propto (1/x)^\lambda$, are shown together with the data at indicated Q^2 values. The full line shows the fit in the range $x < 0.01$, the dotted line in the range $x < 0.001$. The dots show the data with error bars given by the statistical and systematical errors added in quadrature. In the fit, all correlations of errors were taken into account.

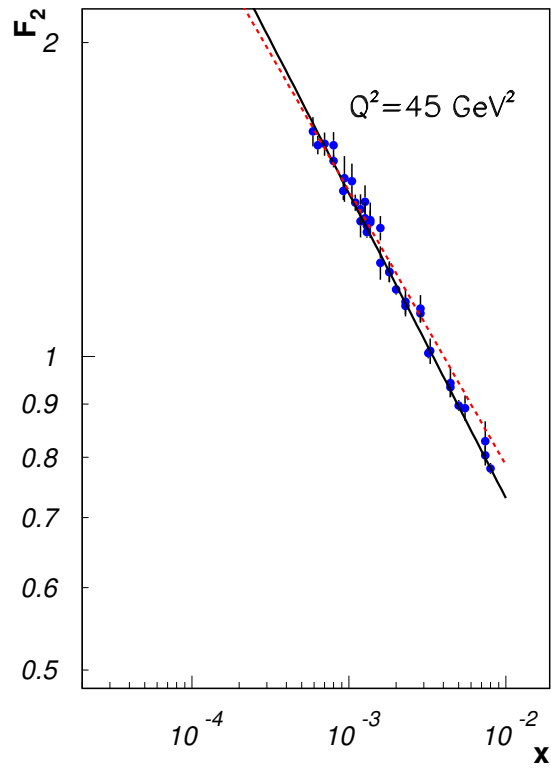


Figure 9: The fitted curves, $F_2 \propto (1/x)^\lambda$, are shown together with the data at indicated Q^2 values. The full line shows the fit in the range $x < 0.01$, the dotted line in the range $x < 0.001$. The dots show the data with error bars given by the statistical and systematical errors added in quadrature. In the fit, all correlations of errors were taken into account.

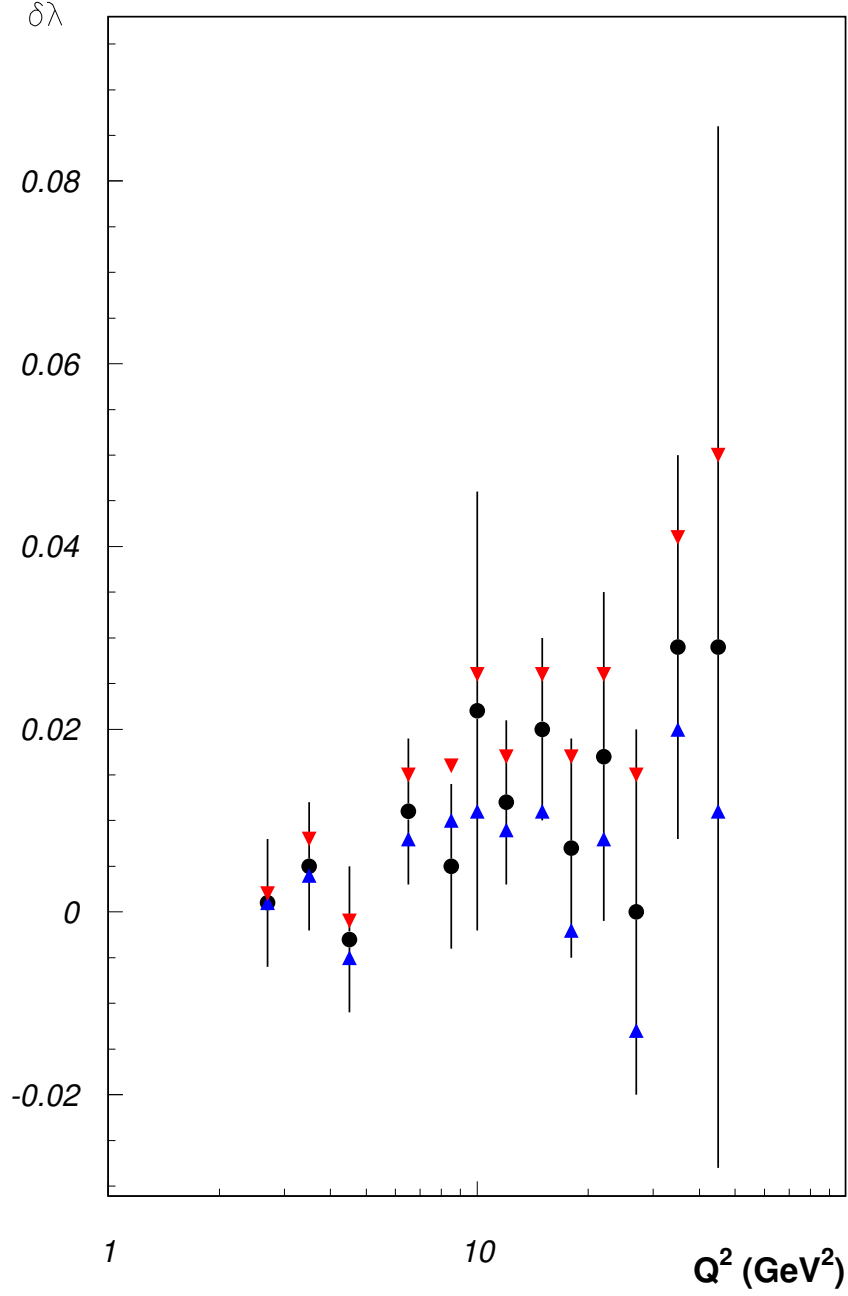


Figure 10: Plot of differences between the values of λ determined in the low- x and very-low- x region, $\Delta_\lambda = \lambda_{x < 0.01} - \lambda_{x < 0.001}$. The black dots show the results for $R = 0.25$, the triangles pointing down show the results for $R = 0.2$ and the triangles pointing up show the results for $R = 0.3$. The errors of black dots were obtained from the quadratic addition of errors, $\delta_{\Delta_\lambda} = \sqrt{\delta_{\lambda_{x < 0.01}}^2 + \delta_{\lambda_{x < 0.001}}^2}$. The errors of the triangles are of about the same magnitude and were not displayed, for clarity.